Combining spectral and spatial information for heavy equipment detection in airborne images

Katia Stankov
R&D department
Synodon Inc.
Edmonton AB Canada
e-mail: katia.stankov@usherbrooke.ca

Boyd Tolton
R&D department
Synodon Inc.
Edmonton AB Canada
e-mail: boyd.tolton@ synodon.com

Abstract - **Unsupervised construction on the pipeline right-of-way may provoke pipe rupture and consequently gas leaks. Heavy equipment is seen as a clue for construction activity. Monitoring the pipeline right-of-way for heavy equipment is therefore important for environmental and human safety. Remotely sensed images are an alternative to expensive and time consuming foot patrol. Existing image processing methods make use of previous images and/or external data. Both are not always available. We propose a new method for image processing to detect heavy equipment without the need of auxiliary data. We first detect potential heavy equipment locations and then use spatial descriptors and spectral information to eliminate false alarms. The method was validated in different environments – urban, vegetation, open excavation – and in different seasons. The experiments demonstrated the capacity of the method to detect heavy equipment without the use of previous images and/or external data.**

Keywords-remote sensing image processing; right-of-way threats detection; differential morphological profile; spectral information; Hausdorff distance.

I. INTRODUCTION

Unsupervised construction activity on oil and gas pipeline's Right-of Way (ROW) may lead to pipeline rupture and leaks. The periodic surveillance of the ROW for the presence of heavy equipment or construction machinery, referred also as ROW threats, is therefore vital to protect the human safety and to prevent ecological damage. Pipeline networks span thousands of kilometers and may be located in remote and difficult to access areas. Airborne and satellite images are considered to complete the surveys. Computer based methods to detect construction machinery in these images represent an alternative of the slow and tedious task of visual image analysis.

In our previous paper [1] we presented a method for heavy equipment detection in airborne images, based on the differential morphological profile and spatial characteristics of the objects. In this paper, we present a notable improvement of the method by analyzing spectral information as well. We have also shown expanded experiments to support the method's achievements.

The paper is organized as follows. In Section II we give the state-of-the-art, Section III presents the methodology, in Section IV we provide results, validation and discussion, and in Section V a conclusion.

II. STATE-OF-THE-ART

The automation of the process of heavy equipment detection in airborne images faces difficulties from different origin: great variety of vehicles; uneven flight altitude; different view and orientation of the images; variable illumination conditions; occlusion by neighboring objects, and others [2]. In addition, construction vehicles are sometimes very similar to transportation vehicles. All these make the development of pattern recognition algorithms for ROW threat detection a challenging remote sensing image processing task.

Existing methods extract characteristic features to decrease the differences between construction vehicles (decrease the intra-class heterogeneity), while increasing the inter-class heterogeneity, i.e., make heavy equipment more distinguishable from other objects. In [3], scale-invariant feature transform was applied on previously defined scale invariant regions to receive object descriptors and detect vehicles. Presuming that local distribution of oriented gradients (edge orientations) is a good indicator for the presence of an object, Dalal [4] proposed the accumulative Histogram of the Oriented Gradients (HOG). In [5], the authors mapped HOG to Fourier domain to achieve rotation invariance and used kernel Support Vector Machine (SVM) to classify the data and identify construction vehicles. Using local textural descriptors and adaptive perception based segmentation, the authors in [2] sequentially eliminate background objects from the image, such as buildings, vegetation, roads, etc. The remaining potential threat locations are divided into several parts to extract and evaluate descriptive features and match them against template data. Extraction of local phase information allowed the separation between structure details and local energy (contrast) [6]. Afterwards, based on previously defined image template, the authors in [6] created a voting matrix to detect construction vehicles. An interesting approach to derive the template images from the processed image itself was proposed in [7]. The authors created an immune network and first trained image areas against vehicles samples; next, they processed the whole images in a similar way to detect vehicles. However, the vehicles samples were defined by human operator. Potential vehicle locations were derived through rule based classifier applied on numerous spatial and gray-level features computed on a segmented image in [8]. Statistical classifier was then used to assign

objects to the vehicle class. Though this method avoids the definition of template images, it involved manual image analysis to design training samples.

Exploiting the fact that heavy equipment has a larger number of right corners than natural objects, the authors in [9] defined target and background templates from the images. They used Harris corner detector to perform a first fast processing of UAV images and to reject background. In the second stage of the method the authors compared the performance of four classifiers (k Nearest Neighbors, Support Vector Machine, Decision Trees and Random Tress) and two feature extraction algorithms (HOG and Gabor coefficients). Best results were achieved with Gabor coefficients and Random Trees classifier. However, the results were more consistent while using a set of indoor images of model vehicles, taken in a sand box, than with the set defined from the images.

To decrease the large sets of templates needed to train and test the classifier, the authors in [10] developed a novel system based on the AdaBoost classifier. They applied it on SAR images to detect three types of vehicles and achieved recognition rates above 95% with a very limited training set. Gabor wavelet of SAR images was used to extract descriptive feature parameters in [11] to identify several types of vehicles.

Synthetic aperture radar images provide all weather coverage and are not restricted to the presence of daylight illumination. This property proved very efficient for change detection and potential threat localization [12]. Additional high spatial resolution optical images are to be analyzed to identify positive alarms.

To fully avoid the need of image template, potential threats locations are assessed with the aid of change detection in [13], next auxiliary data is used to decide upon the presence of a threat.

A common trait of existing methods is that the successful recognition of heavy equipment is impossible without complete set of image templates, previous images, and/or auxiliary data. These are not always available in practice. Airborne images of the pipeline ROW are taken only when a customer orders a survey. Previous images are not available when it comes to a new customer. Acquiring auxiliary data or building complete set of templates for the large variety of heavy equipment vehicles will significantly increase the cost of the survey. All of the above made existing methods not applicable in our case, thus we opted for a method that involves the interpretation of individual images.

The new methodology for heavy equipment detection we present in this paper avoids both the need of template images, and the need of auxiliary data or previously acquired images. In addition to increased flexibility, it also makes the performance of the method independent of the quality of the external data. As in our previous method [1], we first localize potential threats by detecting areas of high frequency of the image that correspond to the size of construction machinery and compute spatial descriptors. Unlike the previous method, where we used all the descriptors at once to discriminate between threats and other objects, here we consecutively eliminate non threats locations. The significant improvement of the recognition came from the inclusion of spectral information. We analyze spectral information on the inner parts of the potential locations retained in the previous steps to refine the results. In the following section we give a step by step description of the method.

III. DESCRIPTION OF THE METHOD

The method may be roughly divided in three parts. First, we find potential threat locations. In the next step these locations are treated as objects, and spatial indices are derived to eliminate the ones that are certainly no threats. Finally, we introduce spectral information to further tune the results. A detailed description is given in Fig. 4.

A. Finding potential threat locations

To build our method we take advantage of the fact that construction vehicles have non-flatten surfaces, which creates inequality in the intensity of surface pixels and together with their outer edges make that they appear as areas of high frequency in the image. Therefore, potential threat locations may be found by identifying areas of high frequencies that are in the range of heavy equipment size. We apply the differential morphological profile on the gradient of the image to find areas of high frequency.

1) Differential Morphological Profile (DMP): DMP is an iterative algorithm that performs opening/closing by reconstruction with a structuring element (SE) to find structures that are brighter/darker than their surroundings. The size of the SE is increased in the consecutive iteration and the result is extracted from the result of the previous iteration. As we are searching for structures that are brighter than their surroundings, we used only the opening by reconstruction to compute the DMP, as follows [14]. Let the vector $\Pi\gamma(x)$ be the opening profile at the point x of image I defined by:

$$\Pi\gamma(x) = \left\{\Pi\gamma_\lambda : \Pi\gamma_\lambda = \gamma_\lambda^*(x), \forall\lambda \in [0,...,n]\right\} \quad (1)$$

where $\gamma_\lambda^*(x)$ is the morphological opening by reconstruction operator and the size of the $SE = \lambda$.

The DMP $\Delta\gamma(x)$ is a vector that stores a measure of the slope between consecutive iterations of the opening profile corresponding to the increased size of the SE:

$$\Delta\gamma(x) = \left\{\Delta\gamma_\lambda : \Delta\gamma_\lambda = \left|\Pi\gamma_\lambda - \Pi\gamma_{\lambda-1}\right|, \forall\lambda \in [1,...,n]\right\} \quad (2)$$

When the SE size exceeds the object size, the background intensity values are assigned to the object. Thus, by extracting two consecutive results, bright objects that correspond or are bigger than the size of the corresponding SE are retained. The object is eliminated in the consecutive iteration if it is smaller than the SE. Thus by knowing when,

in what level of the DMP, an object disappeared one may conclude about its size.

The DMP has to be applied on a grayscale image, usually the brightness (the maximum between the red, green and blue channel - RGB) is used. Here we introduce a new technique based on the Color Invariant Model developed by Gevers and Smeulders [15].

2) Invariant Color Model: The invariant color model computes the angles of the reflection vector and is invariant to illumination intensity and viewing direction [15].

$$C1 = \arctan(R/\max\{G,B\}) \quad (3)$$

$$C2 = \arctan(G/\max\{R,B\}) \quad (4)$$

$$C3 = \arctan(B/\max\{R,G\}) \quad (5)$$

The model was designed to compensate for matte and dull surfaces and increases the differences in the inner parts of the construction machinery, which are sometimes attenuated in RGB. To enhance these inequalities, we generate a new image using the maximum between C1, C2, and C3, and compute the gradient of this image.

The gradient of an image measures the directional changes of the intensity levels of an image. Because these changes are greater towards the edges of an object, the gradient highlights the transitions between objects. The uneven surface of heavy equipment may be related to as composed from few small objects, which in the gradient image generated from the invariant color model will appear as a high concentration of edges.

3) Computing the gradient: To obtain the gradient of the image we use the measure of the discontinuity D_{xy} at each pixel with image coordinates x and y [16]:

$$D_{xy} = \sqrt{G_x^2 + G_y^2} \quad (6)$$

where G_x and G_y are the gradients at an image pixel in the x (horizontal) and y (vertical) directions, respectively. To compute the gradient we approximated the partial derivative in the horizontal direction with the central difference between columns; and in the vertical direction – with the central difference between rows, based on Sobel kernel.

As shown in Fig. 1, the gradient of the image derived from the invariant color model produces an aggregation of edges in the inner parts of the threats, which allow for better differentiating construction machinery from other vehicles, compared to the gradient obtained from the brightness image. The higher the gradient value of a pixel, the higher the possibility that it belongs to an edge. To retain edges we threshold the gradient image derived from the invariant color model using the Otsu's method.

4) Localizing areas of high frequency: To find areas of high frequency we applied the DMP on the gradient image. The separation between objects with DMP depends on the size of the SE used for the opening by reconstruction [17]. To fit inner parts of heavy equipment machinery we derived the set of SEs from the size of these parts in accordance with the spatial resolution of the image. In our case, the size of the image pixel is 9 cm, which allowed using a set of SE ranging from 4x4 to 12x12 pixels with an increment of 4. When using DMP, objects situated closer than the size of the SE may be merged together in the corresponding DMP level. The set of SE we used was kind of compromise between retaining the whole construction vehicle and avoiding the merge with nearby objects. To eliminate irrelevant locations we first used spatial information.

Unlike our previous method where we used all relevant spatial properties simultaneously to apply principal component analysis (PCA) and reduce false positives, here we first eliminated irrelevant locations based on the thresholding of few spatial properties. Next, we introduced spectral information and together with additional spatial property, we used the PCA to further refine the detection. As in the feature space the discrimination between classes is not linear [18] this two steps filtering proved to be more efficient.

B. *Spatial information*

For each DMP level, we find out connected components

(a) (b) (c)

Figure 1. Gradient image. (a) Original RGB (b) Gradient of the brigthness image (from the original RGB); (c) Gradient of the maximum between C1, C2 and C3 (the invariant color model). Heavy equipment is given in red rectangles. The inavriant color model enhances the edges in the inner parts of the heavy euipment, and in result the threats are more distinguishible from other vehicles in (c), compared to (b).

and obtained image objects for which spatial properties may be computed. To each one of the spatial properties we assigned thresholds with a large margin of error in order to ensure only objects that for certain are not threats will be removed. As we further refine the results we were not concerned in this step of the method about the number of false positives. Following is a description of the spatial properties that better discriminate heavy equipment from other objects together with the way we set an appropriate threshold for them:

1) Area: As stated earlier threats may merge with background depending on the interaction between their size and the size of the SE. For example, construction machinery is often situated in areas with digging activity. Digging is characterized by soil piles, which cast shadow and produce edge like effect in images and may merge with nearby objects. Sometimes, the distance between threats may be smaller than the size of the SE and consequently they will merge in the corresponding level of the DMP. As in these cases larger objects will correspond to heavy equipment, we defined a high threshold value for area (10000 pixels) and removed objects above it.

2) Elongation: Heavy equipment has rectangular shape. The ratio between the major and the minor axis length of the object is a good indicator for the rectangularity of a shape. Higher values for this ratio correspond to objects with linear extension such as roads. Square shapes obtain values closer to 1. We gave a large margin between 1.1 and 5.

3) Curvature: We approximate the curvature with the radius of the circle that fits the best the contours of the object. First we fill the objects, next we find the coordinates of the contour of the filled objects to solve the least mean square problem and calculate the radius of the circle. The curvature is given by 1/radius [19]. The curvature of a straight line will be zero, so the greater the ratio 1/radius, the greater the curvature of the curve. We are searching therefore for objects whose curvature is greater than 0 and lower than some value corresponding to curved shapes. As we eliminate lines based on the elongation property we are not concerned to impose a lower threshold to the curvature. To define an upper threshold we use the Hough transform.

4) Hough transform: Hough transform is useful technique to fit straight lines to object boundaries. For small round objects it finds zero lines. We use the Matlab implemented algorithm with the only constraint of 100 peaks in the parametric space, and find the minimum curvature of the objects that received no lines after the Hough transform. We use this minimum curvature value of the most curved objects in the image to define an upper threshold on the curvature.

To further refine the results and decide whether an object belongs to the class of heavy equipment we analyzed also spectral information.

C. Assigning objects to the class of heavy equipment

To assign objects to the class of heavy equipment we use spectral information, vegetation mask, and a property called edgeness. We designed decision rules to determine whether an object may represent a threat.

1) Spectral properties: We analyze spectral information derived from the inner parts of the objects because the spectra of their contours may be affected by the transition between objects and therefore not a good indicator of the spectral properties of the object. As heavy equipment is painted in saturated colors it appears as bright spot in at least one of the invariant color bands C1, C2, and C3, and as dark spots in the remaining bands, on the contrary of other manmade objects or the background, which have average values in all of the channels. We generate two images; one

(a)

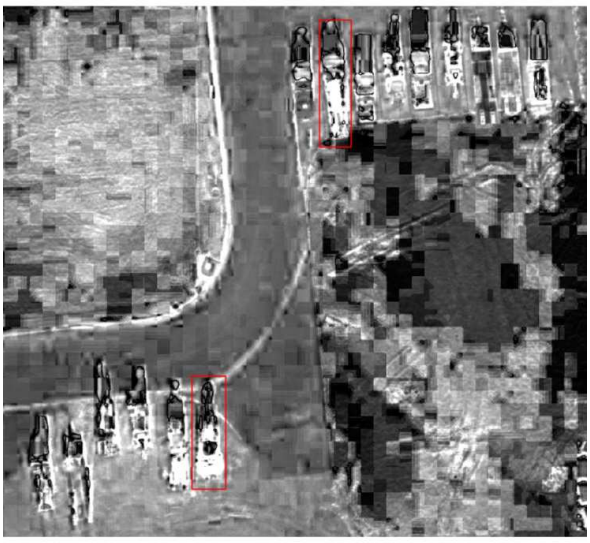

(b)

Figure 2. Images used to compute the Hausdorff distance. (a) Minimum pixel value between C1, C2 and C3 (the invariant color model); (b) Maximum pixel value. In the red rectangles are given examples of heavy equipement. Lower values in (a) correspond to higher values in (b).

takes the minimum between the three new channels for each pixel (Fig. 2 (a)) and the other one – the minimum (Fig. 2 (b)).

To assess the differences between the maximum and minimum of the set of pixels occupying the inner parts of objects, we use the Hausdorff distance. It is an efficient measure to estimate the mismatch between two sets of points without being influenced by variance or noise [20].

Given two sets of points A = {a_1, …., a_n} and B = {b_1, …., b_n}, the Hausdorff distance is defined as [20]:

$$H(A,B) = \max(h(A,B), h(B,A)) \quad (7)$$

where

$$h(A,B) = \max_{a \in A} \min_{b \in B} \| a - b \| \quad (8)$$

and ||.|| is some norm. We used the Euclidean distance.

The Hausdorff distance first identifies the point of given set A that is farthest from any point in set B and then computes the distance from this point to its nearest neighbor in B and vice versa, from the point of B that is farthest from any other point of A, it finds the distance to the nearest neighbor in A. Then it takes the maximum between the two distances. Thus, every point in one set is within the Hausdorff distance from some other point in the other set and vice versa [20].

We calculate the Hausdorff distance between the two sets of pixels values obtained from the maximum and minimum images received from the C1, C2, and C3 bands. As heavy equipment vehicles have saturated colors they will receive higher values for the Hausdorff distance. Moreover, a larger amount of their pixels will reside within this margin, according to the per pixel difference between the maximum and the minimum of the C1, C2, and C3 channels. We compute the percent of pixels in the whole object whose differences between the maximum and the minimum of the C1, C2, and C3 channels are within the Hausdorff distance for the corresponding object. In the rest of the paper we refer to this property as spectral mismatch occupancy (SMO). Construction machinery receives higher SMO values, as most of the pixels are in the margins defined by the Hausdorff distance. Would we define a threshold on the saturation image to compute the SMO, we would receive higher values for other objects too. We illustrate this in Fig. 3. As shown, the Hausdorff distance allowed to better differentiate the levels of saturation.

To define whether an object may belong to the class of

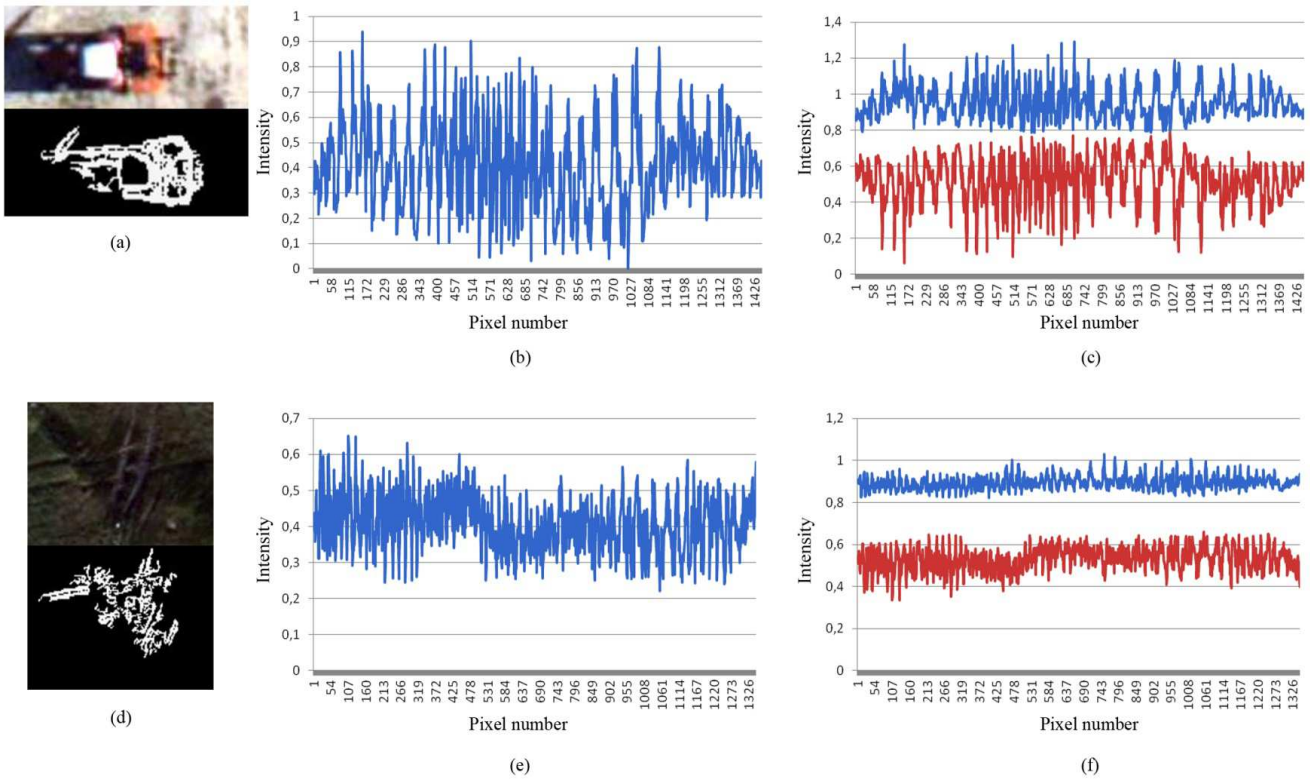

Figure 3. Saturation versus Hausdorff distance: (a) Heavy euqipment, original RGB (above), corresponding object (below); (b) Saturation profile of the object in (a); (c) Maximum and minimum profile of the object in (a); (d) Background object, original RGB (above), corresponding object (below); (e) Saturation profile of the object in (b); (f) Maximum and minimum profile of the object in (b). For the heavy equipment in (a) the Hausdorff distance is equal to 0.59, the SMO is 0.24. For the object in (d) Hausdorff distance equals 0.52, SMO – 0.2.

heavy equipment we compare the SMO to the vegetation occupancy.

2) Compare SMO to vegetation occupancy and apply decision rules: First, we compute the vegetation index from the RGB bands, because the airborne images we work with have only these three bands:

$$Vegetation\ Index = (Green - Red)/(Green + Red) \quad (9)$$

Using the Otsu's threshold method, we generate a vegetation mask. The vegetation occupancy of an object is obtained as the percent of masked pixels in the object area.

The difference between SMO and vegetation occupancy varies according to the scene. To adapt our method we apply the following rules to retain ROW threats.

In scenes occupied mostly by green vegetation, a single threat will have definitely higher SMO than vegetation occupancy, compared to other objects. Thus, if less than 10 percent of the objects have higher SMO than vegetation occupancy, we assume that this is the case and retain these objects (Fig. 6 (a)). However, when the scene is occupied by buildings, excavations, or the image is taken in winter season when no green vegetation is present, but only leafless trees and shrubs, the vegetation mask may also cover part of the heavy equipment and the predominance of SMO over vegetation occupancy is not so evident.

In cases where there is a lack of strict distinction between vegetation and other objects (the SMO is less than the vegetation occupancy for all of the objects or more than 10 percent of the objects have higher SMO than vegetation occupancy), we use the property called edgeness. It is obtained by dividing the area of the object by the number of edge pixels of the object. To receive the area of the object we fill the boundary of the object. As stated earlier, because of the surface inequalities of construction vehicles, they will receive higher edgeness than vegetation areas, or other transport vehicles as shown in Fig. 1 (c).

We concatenate the two properties: 1) the difference between SMO and vegetation occupancy; 2) the edgeness value. Then we computed the principal component analysis and divided the objects according to their first principal score, setting the median of the scores as a threshold. To decide which group to retain we used the ratio between the eigenvalues of the covariance matrix of each group. Threats have higher intra-class heterogeneity compared to other objects. The ratio between the eigenvalues is a good indicator for heterogeneity [21], thus we used the ratio of the eigenvalues of the covariance matrix. Greater values correspond to greater heterogeneity, thus we retained the group that produced higher value for the eigenvalue's ratio.

Step by step results together with a flow chart of the method are given in Fig. 4.

D. Post-processing

As the images may not contain threats at all, we included a step of automate post-processing to refine the results. We used a vector composed from the Hausdorff distance and the SMO. We then sorted the magnitude of the vector and computed the slope of the tangent at each point. A point

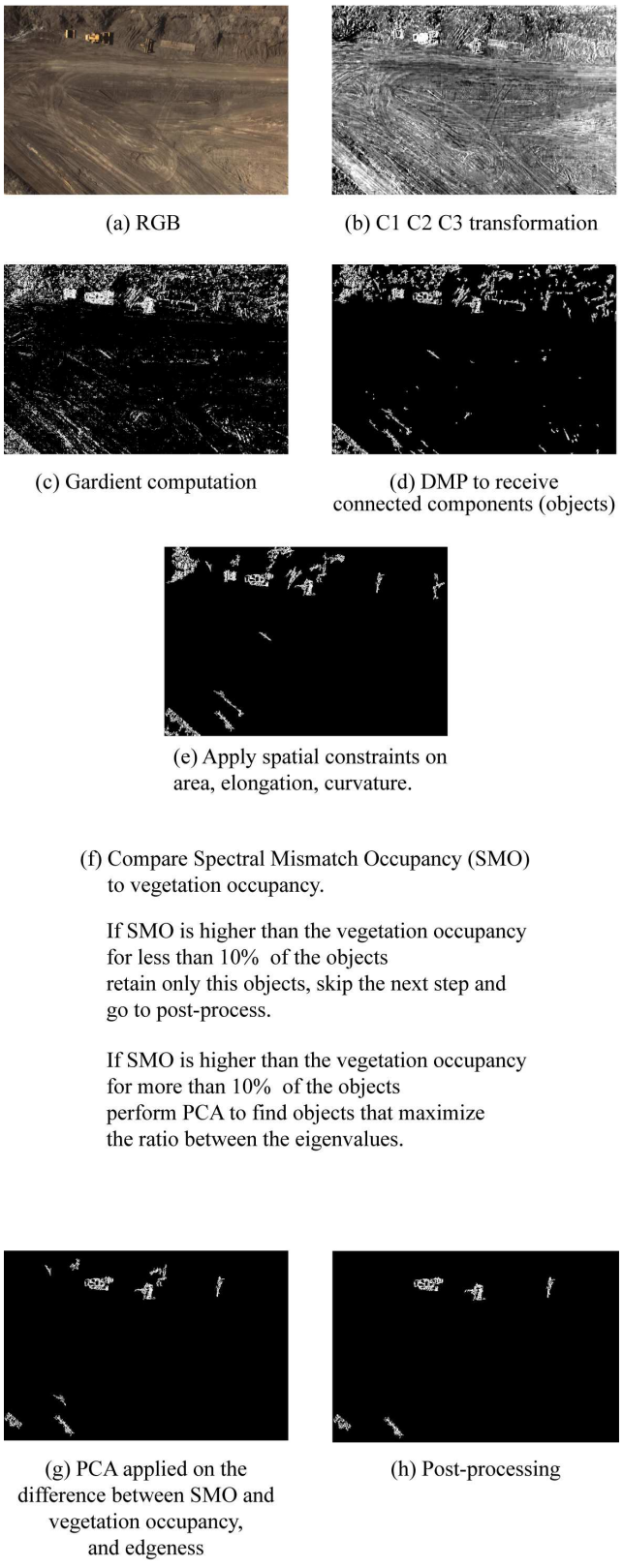

Figure 4. Flow chart of the proposed method. From (a) to (h) - the consecutive steps.

represents the sorted magnitude value for each object. An empirically derived threshold was set to retain objects whose slope was less than the threshold. The rationale here is that if the objects belong to the class of threat their magnitude will be similar and therefore the slope of the tangent will be less than this ratio. If no threat were retained the values for the magnitude will be quite different and the slope will be higher than the threshold. As shown in Fig. 5 this step was efficient to further refine the results.

IV. RESULTS AND VALIDATION

We present some results in Figs. 6, 7 and 8. We indicated true detections – heavy equipment that are present in the image and were identified by the method – with rectangles with yellow contours; false alarms, or false positives – objects that were identified by the method as threats, but are actually not threats – with rectangles with red contours, and missed detection – heavy equipment that is present in the image but was not identified as such by the method – with rectangles with green contours.

As may be seen from Fig. 6 the method performs well in different scenes – forest (a), urban scene (c), abandoned site (e), and ongoing excavations (g). These different backgrounds provide low (abandoned site – (e)) to high contrast (ongoing excavations – (g)). Despite that, the method successfully detected ROW threats. We explain this with the improved spectral contrast obtained with the invariant color model. In Fig. 6 (c) many transportation vehicles were present, which are usually a source of confusion with heavy equipment. The edgeness property allowed for better separation between them. Similar results are shown in Fig. 7 ((a) and (e)).

Fig. 7 (c) shows a typical case of missing a threat. Although both vehicles are very similar, only one was detected. The other one was merged with the nearby fence and treated as a linear object. Fig. 7 (g) demonstrates the capacity of the method to detect threats when there is an accumulation of objects with size similar to this of heavy equipment, that appear as areas of high frequency. However, in this case, many false alarms were also detected as threats.

In Fig. 8 we demonstrate the limitation of the method. When a single threat is present in the image, other objects may be misinterpreted as threats and the real threat omitted. In our opinion, the main reason for this is that while performing the PCA we assume the presence of only two classes. This may be improved by using cluster analysis, applied on the objects principal component scores. In Fig. 8 (c, e and g) we demonstrate typical cases of false alarms. We believe that more rigorous post- processing step would decrease their number.

To validate the accuracy of the method we compared the results to manually detected threats. We refer to the latter as ground truth data. A set of 300 images taken from different surveys was processed. The image size is 1200x800 pixels with average pixel resolution of 9 cm. The detection rate was 83.9% - heavy equipment machines that are present in the ground truth data and were detected by the algorithm. This is a slight improvement compared to our previous method, where the detection rate was 82.6%. However, in the current experiment the images are more heterogeneous, taken from different seasons, as opposite to the previous test where we used images of the same flight day. Also, visual comparison reveals that the number of false positive was significantly reduced.

To place our method among other algorithms for threat detection we compare its achievement to the results reported in [9]. The authors compared several classifiers. Our method, with the detection rate of 83.9% performs slightly better than the kNN classifier (83.3%) and less than the regression trees and SVM classifiers – 85.7% and 93.3%, respectively. However, these classifiers were applied on rural scene only and used template models. As we demonstrated above, our method performs well in different scenes, without using templates or auxiliary data. We may say therefore that it has a potential and we focus our further developments to improve the detection rate and reduce the false detections.

At this stage of the development of the algorithm we are less concerned with the rate of false recognition, as the results are reviewed by an operator. We consider including additional descriptors to reduce the number of false positives events while increasing the detection rate.

The limitation of the method is related to the spatial resolution of the image. In our opinion, the method performance may decrease when applied on images with much lower spatial resolution, more than 1 meter for example, as it relies explicitly on information taken from an increasing neighborhood.

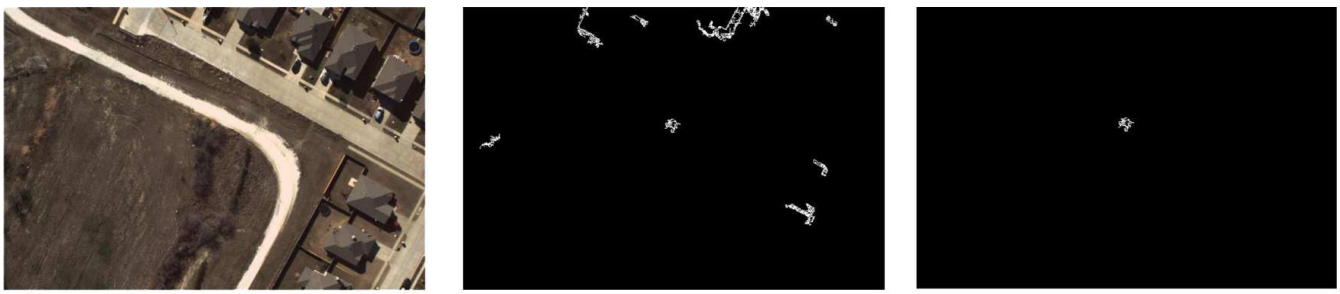

(a) (b) (c)

Figure 5. Post-processsing. (a) Original RGB; (b) Processed image; (c) Results after post-processing.

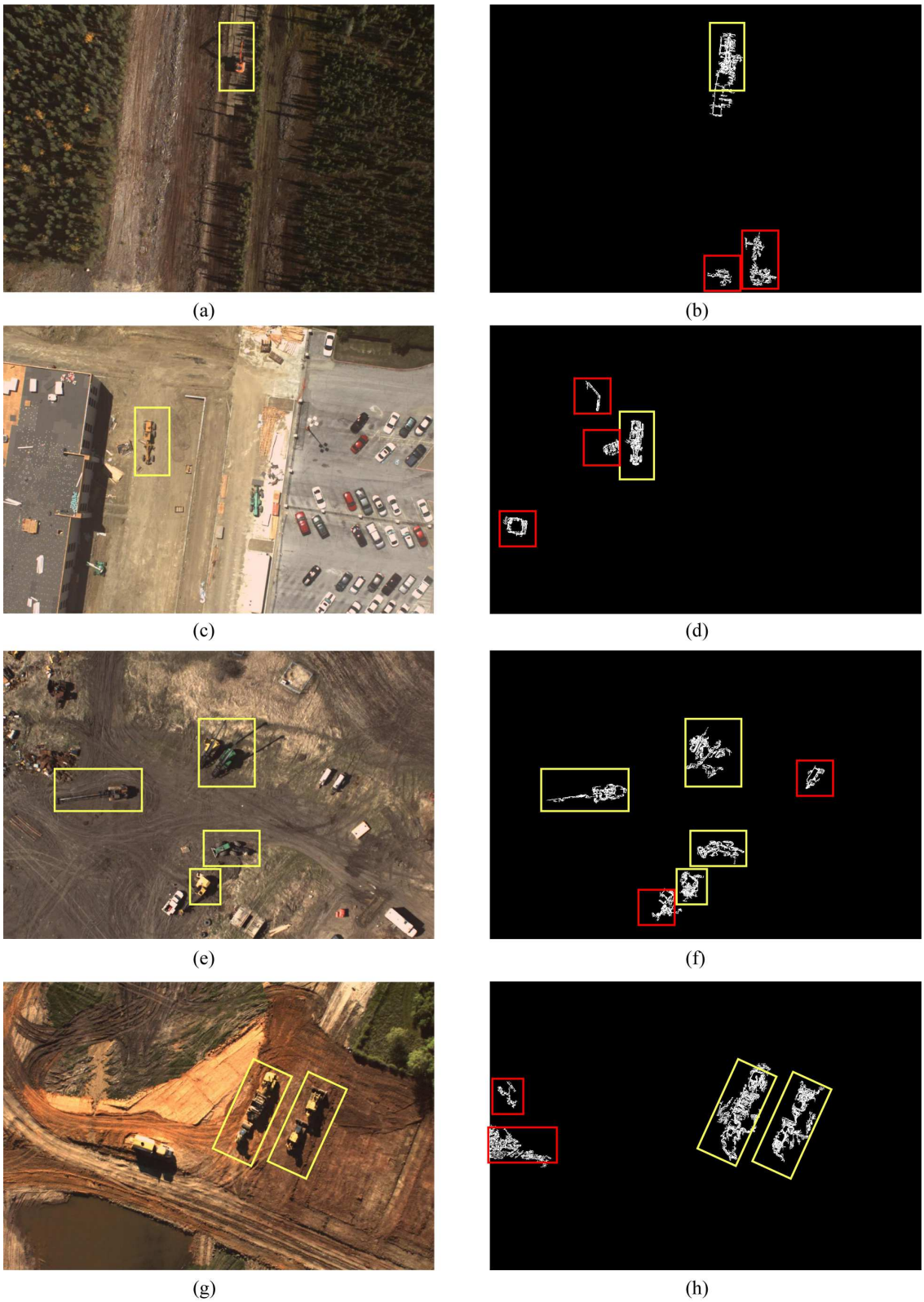

Figure 6. Results. Left column original RGB image. Righ column – detection. Rectangles with yellow contours indicate true detections; rectangles with red contours - false alarms; rectangles with green contours - missed detections.

Figure 7. Results. Left column original RGB image. Righ column – detection. Rectangles with yellow contours indicate true detections; rectangles with red contours - false alarms; rectangles with green contours - missed detections.

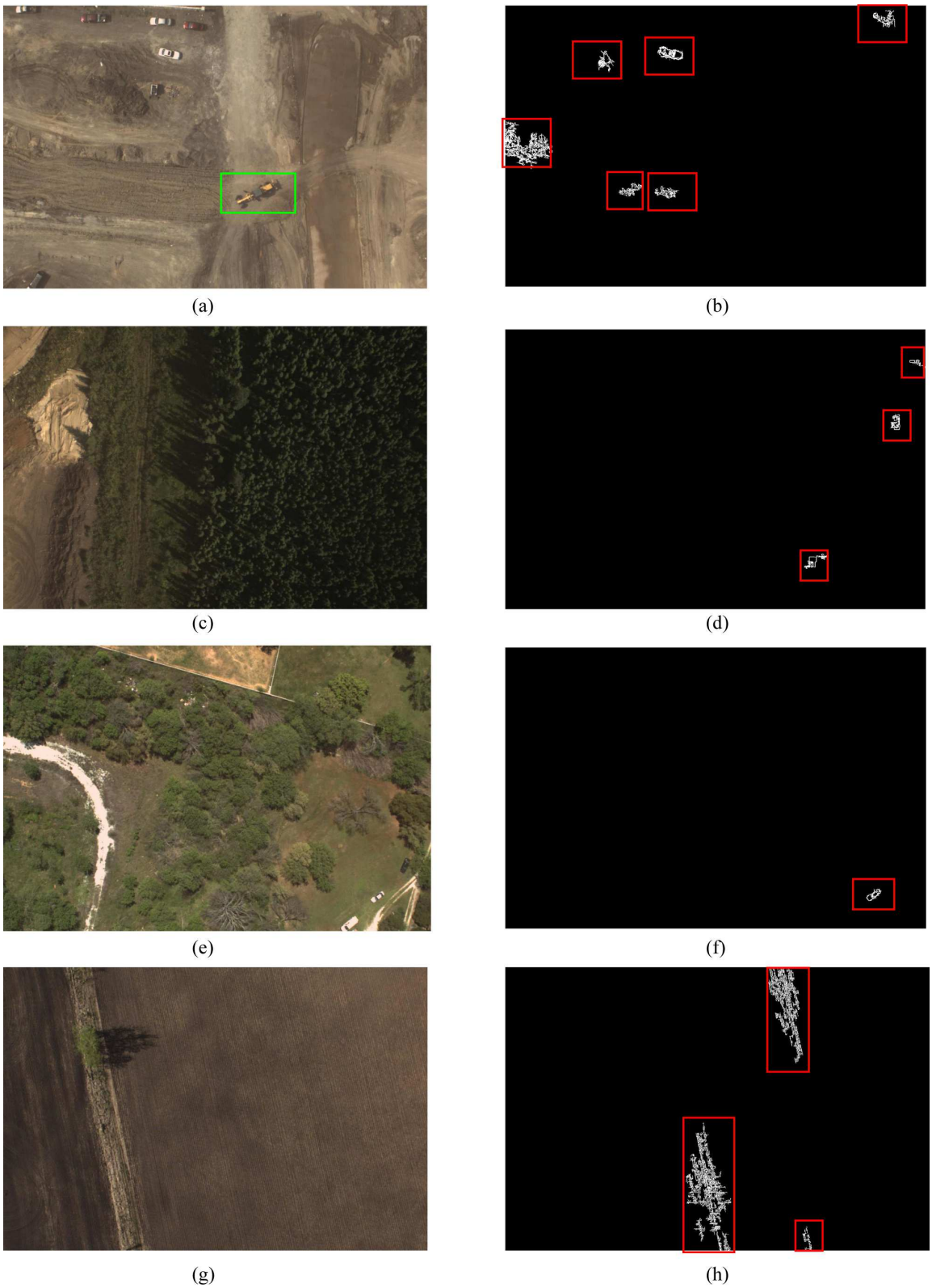

Figure 8. Results. Left column original RGB image. Righ column – detection. Rectangles with yellow contours indicate true detections; rectangles with red contours - false alarms; rectangles with green contours - missed detections.

V. CONCLUSION

In this paper, we presented a novel methodology for heavy equipment detection. The method first detects high frequency areas in the image that may represent potential heavy equipment locations, and then compute spatial descriptors and explore spectral information to eliminate false detections. It does not involve the use of external data, or previously acquired images, which makes it more flexible, compared to already existing algorithms. An improvement compared to our previous method [1] is due to the exploration of spectral information all along the spatial descriptors. Our method compares favorably to other methods for threat detection. On the contrary of other studies, we tested it in different scenes – urban, forest, excavation areas. The experiments proved its efficiency for surveillance of the pipeline ROW, which is important for human safety and ecological damage prevention. The results are promising and we believe that the method has the potential to replace the manual processing of the images.

ACKNOWLEDGMENT

This research was funded by Alberta Innovates Technology Future. The authors would like to express their gratitude for the support provided by the Industry Associate Program of the institution.

REFERENCES

[1] K. Stankov and B. Tolton, “Differential morphological profile for threat detection on pipeline right-of-way. Heavy equipment detection,” The Eighth International Conference on Advanced Geographic Information Systems, Applications, and Services (Geoprocessing 2016), IARIA, Apr 2016, pp. 76-77, ISSN: 2308-393X , ISBN: 978-1-61208-469-5.

[2] V. Asari, Vijayan, P. Sidike, C. Cui, and V. Santhaseelan. "New wide-area surveillance techniques for protection of pipeline infrastructure," SPIE Newsroom, 30 January 2015, DOI: 10.1117/2.1201501.005760

[3] G. Dorko and C. Schmid, “Selection of scale-invariant parts for object class recognition,” IProceedings of the 9th International Conference on Computer Vision, Nice, France, pp. 634–640, 2003.

[4] N. Dalal and B. Triggs, ”Histograms of oriented gradients for human detection,” IEEE Conference on Computer Vision and Pattern Recognition, pp. 886-893, 2005

[5] A. Mathew and V. K. Asari, ”Rotation-invariant Histogram Features for Threat Object Detection on Pipeline Right-of-Way,” in Video Surveillance and Transportation Imaging Applications 2014, edited by Robert P. Loce, Eli Saber, Proc. of SPIE-IS&T Electronic Imaging, SPIE vol. 9026, pp. 902604-1-902604-1, 2014 SPIE-IS&T doi: 10.1117/12.2039663

[6] B. Nair, V. Santhaseelan, C. Cui, and V. K. Asari, “Intrusion detection on oil pipeline right of way using monogenic signal representation,” Proc. SPIE 8745, 2013, p. 87451U, doi:10.1117/12.2015640

[7] H. Zheng and L. Li, “An artificial immune approach for vehicle detection from high resolution space imagery,” IJCSNS International Journal of Computer Science and Network Security, vol.7 no.2, pp. 67-72, February 2007.

[8] L. Eikvil, L. Aurdal, and H. Koren, “Classification-based vehicle detection in high resolution satellite images,” ISPRS Journal of Photogrammetry and Remote Sensing, vol. 64, issue 1, pp. 65-72, January 2009. doi.org/10.1016/j.isprsjprs.2008.09.005

[9] J. Gleason, A. Nefian, X. Bouyssounousse, T. Fong, and G. Bebis, “Vehicle detection from aerial imagery,” 2011 IEEE International Conference on Robotics and Automation, pp. 2065-2070, May 2011.

[10] Y. Sun, Z. Liu, S. Todorovic, and J. Li, “Synthetic aperture radar automatic target recognition using adaptive boosting,” Proceedings of the SPIE, Algorithms for Synthetic Aperture Radar Imagery XII, 5808, pp. 282-293, May 2005.

[11] P. Vasuki and S. M. M. Roomi, “Man-made object classification in SAR images using Gabor wavelet and neural network classifier,” Proc. IEEE. Devices, Circuits and Systems Int. Conf., India, pp. 537–539, IEEE 2012.

[12] Roper, W. E. and Dutta, S. "Oil Spill and Pipeline Condition Assessment Using Remote Sensing and Data Visualization Management Systems,” George Mason University, 4400 University Drive, 2006.

[13] M. Zarea, G. Pognonec, C. Schmidt, T. Schnur, J. Lana, C. Boehm, M. Buschmann, C. Mazri, and E. Rigaud, “First steps in developing an automated aerial surveillance approach,” Journal of Risk Research, vol.13(3–4): pp. 407–420, 2013 doi:10.1080/13669877.2012.729520.

[14] J. A. Benediktsson, M. Pesaresi, and K. Arnason, “Classification and feature extraction from remote sensing images from urban areas based on morphological transformations,” IEEE Transactions on Geoscience and Remote Sensing, vol. 41(9), pp. 1940–1949, 2003.

[15] T. Gevers and A. W. M. Smeulders, “Color based object recognition,” Pattern Recognit., vol. 32, pp. 453–465, Mar. 1999.

[16] H. Wang and D. Suter, “Color image segmentation using global information and local homogeneity,” in: Proc. VIIth Digital Image Computing: Techniques and Applications, Sun C., Talbot H., Ourselin S. and Adriaansen T., Eds., Sydney, pp. 89-98, Dec. 2003.

[17] G.K. Ouzounis, M. Pesaresi, and P. Soille, "Differential area profiles: decomposition properties and efficient computation,” IEEE Transactions on Pattern Analysis and Machine Intelligence, vol. 34, no. 8, pp. 1533-1548, Aug. 2012.

[18] X. Chen, T. Fang, H. Huo, and D. Li, “Graph-based feature selection for object-oriented classification in VHR airborne imagery,” IEEE Transactions on Geoscience and Remote Sensing, vol. 49 (1), pp. 353–365, 2011.

[19] https://www.mathworks.com/matlabcentral/newsreader/view_thread/152405

[20] D. P. Huttenlocher, G. Klanderman, and W. J. Rucklidge,. “Comparing images using the Hausdorff distance,” IEEE Trans. Pattern Anal. Mach. Intell. 15, 9, pp. 850–863, 1993.

[21] F. O’Sullivan, S. Roy, and J. Eary, “A statistical measure of tissue heterogeneity with application to 3D PET sarcoma data,” Biostatistics vol. 4, pp. 433–448, 2003.